Energy 314 (2025) 134036

Contents lists available at ScienceDirect

Energy

journal homepage: www.elsevier.com/locate/energy

Non-ideal effects assessment on organic vapor compressions using small radial turbocompressors for heat pump-based systems

Andrés Sebastián *, Rubén Abbas, Manuel Valdés

Universidad Politécnica de Madrid (UPM), José Gutiérrez Abascal 2, 28006 Madrid, Spain

ARTICLE INFO

Keywords:
Non-ideal gas flows
Dimensional analysis
Turbocompressors
Vapor compression
Heat pumps

ABSTRACT

Radial turbocompressor-driven heat pumps are currently being fostered for their application in a wide range of novel energy systems. This encourages the development of small centrifugal compressors that use different organic vapors. The present work aims to analyze the dynamical similitude preservation when a given heat pump operates with two different organic vapors (propane and isobutane). Scaling is carried out through an upgraded version of a previously developed similarity-based and generalized flow turbomachinery scaling methodology. Numerical calculations are conducted to quantify the non-ideal effects on key performance indicators. Furthermore, the use and of new dimensionless numbers are discussed, and their influence on scaling is assessed under the conditions of this study. The results show a good degree of agreement between the analytical predictions and the numerical simulation in terms of velocity flow field, polytropic efficiency and total pressure ratio. The findings of this work lead to set out that scaling with a proper non-ideal effects characterization is achieved without any further correction. Finally, this study confirms the suitability of the proposed similarity-based method for small radial turbocompressor-based heat pumps in the analyzed thermodynamic window design space.

1. Introduction

Heat pump-based technologies are aimed to be part of the solution to achieve the increasingly necessary transition towards a low-carbon global energy model [1,2]. There is a wide range of potential technologies such as increased efficiency heat pumps for domestic heating and cooling applications [3], high temperature heating or heating upgrade for industrial purposes [4], waste heat recovery [5], polygeneration systems [6] or even different proposals of pumped thermal energy storage systems [7,8]. Recent advances in research on ultra-high-speed permanent magnets electric motor technology [9] allow the development of compact units based on downsized radial turbocompressors for small-scale applications. As a general classification, radial micro-turbocompressors, also known as micro centrifugal compressors, are those with rotational speed greater than 200 kmin^{-1} and impeller outer diameter less than 30 mm [10]. This is precisely why electrically-driven micro-turbocompressors using working fluids other than air, such as natural refrigerants or organic vapors, are currently being explored for these novel heat pump-based systems at small scale.

One of the main enablers in the research of turbomachinery using non-ideal working fluids was promoted by the increased interest in organic Rankine cycles [11]. Intense research work has been carried out in recent decades devoted to the analysis, design, experimentation and manufacturing of organic axial and radial-flow turbines [12]. Hence, there is ongoing research on the characterization of non-ideal compressible fluid dynamics (NICFD) in subsonic and supersonic turbines [13,14]. In fact, recent studies have been published on the extension of dimensional analysis for turbomachinery operating with dense vapor flows [15]. However, there are still gaps in the general comprehension of turbomachinery beyond typical perfect gas assumptions, such as dimensional analysis and performance laws using organic vapor flows [16].

Research efforts are required as a consequence of the growing trend to study organic vapor compressions [17], instead of expansions, for applications such as those of the aforementioned energy systems. Indeed, the influence of the specific heat ratio or isentropic exponent on similarity conditions and the proposed corresponding corrections on compressor performance indicators have been discussed by Van den Braembussche [18] and Casey and Robinson [19]. In addition, novel similarity methods and corrections were proposed for different working mediums in addition to organic vapors, such as gases under supercritical conditions [20] or noble gases [21]. Similarly, generalized similarity-based methods have been developed that include Reynolds number corrections due to the small size of centrifugal

* Corresponding author.
E-mail address: andres.sebastian@upm.es (A. Sebastián).

https://doi.org/10.1016/j.energy.2024.134036
Received 13 November 2023; Received in revised form 11 April 2024; Accepted 29 November 2024
Available online 10 December 2024

Nomenclature

a	Speed of sound (m/s)
α_{TT}	Total-to-total density ratio (–)
β_{TT}	Total-to-total pressure ratio (–)
D	Characteristic dimension (m)
η	Efficiency (–)
$Ec^{*1/2}$	Modified Eckert number (–)
Γ	Fundamental derivative of gas dynamics (–)
γ	Adiabatic specific heat ratio (–)
γ_{pv}	Real isentropic pressure-volume exponent (–)
k_1, k_2	Compressor performance constants (–)
h	Specific enthalpy (J/kg)
M	Absolute Mach number (–)
M_w	Relative Mach number (–)
$\dot{m}$	Mass flow (kg/s)
μ	Dynamic viscosity (Pa/s)
n	Rotational speed (s^{-1})
p	Pressure (Pa)
$\Pi_{\dot{m}}$	Dimensionless mass flow rate (–)
Π_n	Blade Mach number (–)
R	Specific gas constant (J/kgK)
Re	Reynolds number (–)
ρ	Density (kg/m^3)
s	Specific entropy (J/kgK)
T	Temperature (K)
u	Blade velocity (m/s)
Tr	Traupel number (–)
v	Specific volume (m^3/kg)
Z	Compressibility factor (–)

Acronyms

#1–#4	Operating points numbering
CFD	Computational fluid dynamics
DP	Design point compressor performance
DS	Dynamical similarity
GCI	Grid convergence index
HP	Increased pressure ratio compressor performance
Ib.	Isobutane
OP	Operating point
Pr.	Propane

Subscripts

$0x$	Total/stagnation conditions at x
0	Inlet duct
1	Near impeller leading edge
2	Near impeller trailing edge
3	Diffuser outlet
c	Critical
mxp	mixing plane
p	Polytropic
s	Isentropic
sat	Saturation

compressors [22,23] and evaluate the preservation of similarity tip leakage flow structure [24] using ideal and non-ideal working fluids. The theoretical framework for the analysis of one-dimensional flows of perfect gases is currently extended to the case of non-ideal compressible flows through different studies such as Tosto et al. [25], where the molecular complexity and dense-vapor effects are analyzed in compressible internal flows. Giuffre et al. [26] discussed the effects of fluid molecular complexity on the performance of high-speed centrifugal compressors through the extension of prior work addressed by Rusch and Casey [27]. This work led to further evidence that efficient high-speed centrifugal compressor designs operating with high molecular weight organic fluids featuring pressure ratios up to five at off-design conditions are feasible. All these efforts lead to the concept presented by aus der Wiesche and Reinker [16] for generalized performance laws for organic vapor flow turbomachinery, being specifically used in radial turbocompressors, which calls for the assessment of their method for other working fluids and conditions to check the suitability of the non-ideal effects characterization using scaling laws.

This work aims to numerically analyze dynamical similitude preservation between air and non-ideal organic vapors applied to a small-scale radial turbocompressor under operating conditions for low-temperature lift heat pump applications. The novelty of this work lies in the assessment and improvement of generalized performance laws for organic vapors, evaluating its adequacy when using new similarity numbers better suited to turbocompressors operating near the saturation line. Two different organic fluids (isobutane and propane) at two different compressor operating points will be tested under dynamical similarity conditions. The goal of the manuscript, therefore, seeks to answer the question of how much does the non-ideal behavior of the fluids affect when predicting compressor performance near the saturation line for heat pump applications.

2. Methodology

This section describes the methods and actions developed to carry out the proposed investigation. First, a generalized dimensional analysis is set for organic vapor turbomachinery which will be used to generate operating points keeping dynamic similarity conditions (also named homologous points). Then, the numerical modeling approach is explained along with the definition of the micro-scale radial turbocompressor geometry.

2.1. Dimensional analysis for organic vapor turbomachinery

Generalized flow scaling laws are required when dealing with compressible flow turbomachinery using fluids other than air. As introduced in the previous section, aus der Wiesche and Reinker [16] developed a novel formulation for the dimensional analysis of turbomachinery working with non-ideal fluids, which intends to be valid also for complex fluids (fluids with a behavior far from the ideal) such as organic vapors. This functional relationship based on Buckingham's Π-theorem goes beyond the conventional approach of perfect gas and is expressed in Eq. (1). Total-to-total pressure ratio (β_{TT}) and efficiency (η) are chosen as key performance indicators. The first three dimensionless numbers are formulated as usually found in the literature: the blade Mach number (Π_n), the dimensionless mass flow rate ($\Pi_{\dot{m}}$) and the Reynolds number (Re). Now, two additional similarity dimensionless groups are raised in their formulation. The first is called the modified Eckert number ($Ec^{*1/2}$), which can be replaced by γ-similarity in the case of a perfect gas. This number should be understood as a representation of heat transfer dissipation effects, since its physical meaning come from Eckert number, which relates kinetic energy of the flow and the boundary layer enthalpy difference. Finally, another similarity number is proposed, called the Traupel number (Tr), which takes into account the non-perfectness behavior of the fluid. To this end, this number makes use of the partial derivative of the compressibility factor (Z) along an isentropic compression/expansion process which has been defined as relevant to quantify non-ideal compressible flow [11]. Other generalized formulations, instead, use just the compressibility factor although valuable information of the non-perfectness behavior would be lost. For a perfect gas (or perfect vapor), the expressionTr=0 holds and this dimensionless number can be dismissed.

$$\beta_{TT},\eta = f\left(\frac{nD}{a_{01}},\frac{\dot{m}\sqrt{RT_{01}}}{p_{01}D^2},\frac{\rho nD^2}{\mu},\frac{nD}{(RT_{01})^{1/2}},\rho n^2D^2\left.\frac{\partial Z}{\partial p}\right|_s\right) \tag{1}$$

One may note that neither the ideal adiabatic specific heat ratio ($\gamma = c_p/c_v$) nor the real isentropic pressure-volume exponent (γ_{pv}), see Eq. (2), are taken as independent dimensionless numbers.

$$\gamma_{pv} = -\frac{v}{p}\left.\frac{\partial p}{\partial v}\right|_s = -\gamma\frac{v}{p}\left.\frac{\partial p}{\partial v}\right|_T \tag{2}$$

On this innovative basis which considers modified Eckert and Traupel numbers instead of conventional ideal-gas driven γ-similarity and Z dimensionless numbers, some modifications are proposed in this work. A new reformulation is raised for the sake of a major generalization, as shown in Eq. (3). First, the isentropic stage loading or head coefficient ($\Delta h_{0s}/{a_{01}}^2$) is proposed instead of the direct use of total-to-total pressure ratio. This may improve the characterization of the compression (or expansion when applied to turbines) dynamical similarity preservation, since the isentropic enthalpy rise can be kept as a function of the media speed of sound without any kind of perfect gas assumption. Inlet stagnation conditions (represented by the 01 subscript) are set to all the thermofluid properties considered in the analysis. This includes the use of the stagnation inlet speed of sound in the dimensionless mass flow rate in order to not consider any perfect gas assumption neither in the dimensionless mass flow rate nor in the blade Mach number. Finally, the polytropic efficiency is specified as the other key performance indicator of the formulation.

$$\frac{\Delta h_{0s}}{a_{01}^2},\eta_p = f\left(\frac{nD}{a_{01}},\frac{\dot{m}}{\rho_{01}a_{01}D^2},\frac{\rho_{01}nD^2}{\mu},\frac{nD}{(RT_{01})^{1/2}},\rho_{01}n^2D^2\left.\frac{\partial Z}{\partial p}\right|_s\right) \tag{3}$$

Once the new functional relationship is established, one must set constant dimensionless numbers to find homologous points when varying boundary conditions or working fluid. These conditions set the density and speed of sound, thermophysical properties required for the calculation of the two first dimensionless groups. The calculation of the new homologous rotational speed and mass flow rate is straightforward and depends on the compressor performance reference operating point (Eqs. (4)–(5)). The influence of the third group may be omitted if the Reynolds number is large enough to not fall below the critical threshold under which viscous friction on the boundary layer becomes dominant ($Re \gg Re_c$) [28]. Finally, the modified Eckert and Traupel numbers are selected as the degrees of freedom of the model. Hence, their values will be analyzed and compared to find the potential deviations of the method. Considering that dynamical similarity is preserved, efficiency and dimensionless isentropic enthalpy rise must be maintained, as shown in Eq. (6).

$$\Pi_n = k_1 = f(\text{compressor OP}, p_{01}, T_{01}, \text{fluid}) \tag{4}$$

$$\Pi_{\dot{m}} = k_2 = f(\text{compressor OP}, p_{01}, T_{01}, \text{fluid}) \tag{5}$$

$$\frac{\Delta h_{0s}}{a_{01}^2},\eta_p = f(k_1, k_2, Ec^{*1/2}, Tr) \tag{6}$$

Total-to-total pressure ratio (β_{TT}) can then be analytically calculated using the properties of the real gas data (Eq. (7)) taken from REFPROP database [29]. Furthermore, the parameter total-to-total density ratio (α_{TT}) can also be obtained, which is a good measure of volumetric flow preservation in non-ideal compressible flow dynamics. Preservation of the static density ratio is required to ensure that both flow angles and absolute velocity components are kept constant. Any deviation would lead to a change in the impeller outlet width. According to Van der Braembussche [18], for moderate pressure ratios (up to β_{TT} = 1.5) this adjustment can be omitted and the assumption of identical flow angles and unchanged efficiency may still be acceptable. Furthermore, this is of secondary importance in small-scale turbomachinery, where ensuring high-precision manufacturing tolerances is itself a challenge. Hence, this work does not consider any change in geometry, although α_{TT} and its potential effects will be studied. This fact may entail some limitations when extending this methodology to larger compressors if α_{TT} variations are not controlled.

$$\beta_{TT},\alpha_{TT} = f(\frac{\Delta h_{0s}}{a_{01}^2}, p_{01}, T_{01}, \text{fluid}) \tag{7}$$

The proposed analytical methodology will be applied to a reference geometry of a small-scale turbocompressor designed for using air to generate a set of operating points at different heat pump conditions using non-ideal working fluids. Hence, the novel formulation presented above will generate the boundary conditions required for numerical simulation: stagnation inlet temperature and pressure (imposed) together with the calculated mass flow and rotational speed keeping dynamical similitude. Then, numerical results will be compared to the raised scaling laws to check the non-ideal behavior of the chosen organic vapors under selected conditions.

2.2. Numerical model and reference geometry

The numerical model used for this analysis is an upgraded version of the micro-scale radial compressor model developed in Sebastián et al. [23] using ANSYS-CFX. The reference machine is a one-stage unshrouded air centrifugal compressor consisting of a 20 mm impeller diameter with seven blades and seven splitter blades and a vaneless diffuser. At the design point (DP), the micro-compressor with air as working fluid provides an overall total-to-total pressure ratio around 1.4, rotating at 220 kmin^{-1}. The rotational Mach number referred to stagnation inlet conditions (M_{u2}) is 0.67. A higher pressure ratio operating point, named HP, achieves a total pressure ratio around 1.7 at 280 kmin^{-1}, corresponding to a M_{u2} of 0.85. Further technical data can also be found in previous work, together with experimental validation [30].

The stage modeled is formed by a seventh part of the straight inlet duct, the impeller and a vaneless diffuser passage, providing a reference mesh of 4.8 million cells, with an average cell size of 0.043 mm. The Grid Convergence Index (GCI) proposed by Celik et al. [31] is obtained to determine the error band on the convergence solution (discretization error). Two additional meshes have been studied following the Celik's method: a coarse mesh (2.2 million cells, 0.055 mm average cell size) and a fine mesh (10.9 million cells, 0.032 mm average cell size). The GCI value from the fine grid to the intermediate (GCI_{12}) based on the total-to-total pressure ratio is 0.09%, well below 0.54% of the GCI from the intermediate to the coarse mesh (GCI_{23}). Hence, these very low values allow the use of the reference mesh for this numerical problem ensuring stable and grid-insensitive results. The inlet condition is specified in terms of the total temperature and pressure of the fluid; the outlet sets the mass flow rate. This inlet–outlet configuration provides the best numerical stability. The lateral faces of the fluid domain are defined as rotational periodic boundaries to simulate the full stage, as Fig. 1 shows. Stationary-rotating interfaces were solved by means of the mixing plane approach. Working fluid real properties are characterized using the Aungier–Redlich–Kwong model and κ-ω shear stress transport is the selected turbulence model. Regarding the solver control parameters, both high-resolution advection schemes and turbulence numerics have been applied. The convergence criterion of the root mean square residuals is set to 10^{-5} while ensuring convergence of total-to-total pressure ratio and polytropic efficiency. Table 1 provides an overview of the main characteristics of the numerical model.

As mentioned above, the design working fluid of the reference geometry is air at the inlet design operating point conditions 1 bar and 20 °C. At these conditions, the chord-based Reynolds number falls in the range of 10^4–10^5, resulting in a viscous sublayer thickening where viscous effects are not negligible. This may affect the velocity flow field and Reynolds number corrections must be used if dynamical similarity is sought. In order to provide a reference operating point in

Table 1
Main characteristics of the numerical model used.

Subdomains:	Inlet, impeller & vaneless diffuser
Modeling approach:	Steady-state RANS 1/7th stage
Reference mesh:	4.8 M cells
Mesh independence:	GCI_{12}<0.1%
Stationary-rotating interface:	Mixing plane
Turbulence model:	κ-ω SST
Fluid properties:	Aungier–Redlich–Kwong model
Convergence criterion:	RMS 10^{-5} + β_{TT}&η_p convergence
Boundary conditions:	p_{01}, T_{01}, n, $\dot{m}$ (outlet)

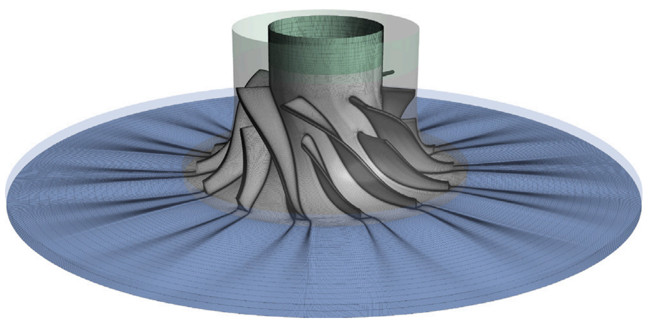

Fig. 1. Meshed view of the numerical model solid parts (inlet, impeller and diffuser) of the reference micro-scale centrifugal compressor geometry.

Table 2
Technical parameters selection of the studied operating points.

	T_{01} (°C)	p_{01} (bar)	Fluids	Compressor OP
OP #1	25	1	Pr. /Ib.	DP/HP
OP #2	10	p_{sat}(5 °C)	Pr. /Ib.	DP/HP
OP #3	30	p_{sat}(25 °C)	Pr. /Ib.	DP/HP
OP #4	50	p_{sat}(45 °C)	Pr. /Ib.	DP/HP

a sufficiently turbulent flow regime, new reference conditions of the inlet air at 5 bar and 20 °C are established applying the design and off-design similarity-based method [23], which has been analytically and numerically validated. Hence, these conditions are the reference for maintaining dynamical similarity through the method proposed in previous Eq. (3). This allows the generation of a set of homologous operating points using organic vapor at any conditions, obtaining the new rotational speed, mass flow rate and inlet pressure/temperature, which are used as inputs for the numerical simulations. The next Section will deal with the selection of the boundary conditions of these new sets using organic fluids.

3. Organic vapors properties and operating point selection

Two low global warming potential and zero ozone depletion potential non-toxic organic compounds have been selected for this analysis: propane and isobutane. These working fluids have been proposed for different environmentally friendly small-scale turbo-heat pump-based energy systems, such as the solar micro-trigeneration system proposed in [6]. The temperature-pressure levels chosen for this analysis are collected in Table 2 for four different operating points (OPs), where T_{01} and p_{01} represent compressor stagnation inlet conditions. All operating points will be studied using both selected working fluids: propane (Pr.) and isobutane (Ib.). In addition, the radial turbocompressor will be studied at two different conditions (DP at M_{u2}=0.67 and HP at M_{u2}=0.85), see the previous Section, in order to analyze two different temperature lifts. Table 2 collects the study set consisting of 16 different calculation points for further numerical validation.

A first set of operating points (#1) are calculated at 1 bar and 25 °C inlet conditions. Although this first set does not correspond to any specific heat pump mode, it may contribute to the understanding of the non-ideal behavior of these organic working fluids. Then, three operating points (#2, #3 and #4) are set in the pursuit of simulating a near-saturation line compression, similar to those compressions for heat pump-like systems. Inlet pressure has been selected in relation to the saturation pressure at 5 °C, 25 °C and 45 °C considering a compressor suction superheat control of 5 K. These boundary condition temperature levels have been selected to represent evaporating lines for heat pumps providing cooling, air heating and heat upgrading, respectively. One may note that mass flow rates and rotational speeds are set according to the preservation of dynamical similarity. Therefore, a total of 16 homologous operating points represent the matrix of the studied cases and will be the object of numerical analysis.

Fig. 2 collects in an enthalpy-entropy diagram the selected operating points for both propane and isobutane working fluids on the different DP and HP compression lines, where temperature contours can also be observed. One may note how the polytropic compression lines Pr. #1 and Ib #1 are represented far from the saturation line with increased specific entropy values. In addition, these plots show the resultant temperature lifts when applied to heat pump-based systems, ranging between 12–20 for propane and 10–18 using isobutane. Although the temperature lifts proposed could be not high enough for some heat-pump based applications, this study aims to explore this thermodynamical region to better understand the compression process of these fluids near the saturation line. If a higher temperature lift is required, one may devise a two-stage (or multi-stage) centrifugal compressor to achieve the desired temperature rise [32,33] or cascade configurations [34]. Nevertheless, there are also low-temperature applications in the range of 10–20 K that can be mentioned, such as domestic geothermal heat pumps or efficient fan coils [35].

These dense vapor compression processes entail a non-perfect thermodynamic behavior due to the proximity of the vapor operating conditions to the saturation lines. This is why compressibility factor contours are shown in Figs. 3(a) and 3(b) for both working fluids chosen, where DP and HP compressor performance operations are displayed. The absolute values of Z are found to be lower when using propane (0.7–0.9) compared to isobutane (0.85–0.95) for the operating points #2–#4, while the operating points under ambient conditions are closer to ideal-gas behavior (Z=1). Fig. 3(c) shows the compressibility factor evolution at isentropic compressions lines for the studied compressors operating points. This plot provides some insight not only on the Z value but also on the $\partial Z/\partial p|_s$ derivative. According to the Traupel classification of fluid mechanics [36], when the fluid flow over an isentropic compression/expansion process provides $Z \neq 1$ but Z can be assumed to be a unique function of the entropy as a single variable Z=f(s) which means that fluid flow motion of a perfect vapor is taking place (e.g. steam). If the compressibility factor cannot be easily obtained by a single thermodynamic variable, its variation over an isentropic compression/expansion line depends on two thermodynamic variables, such as pressure and temperature. This behavior can be considered as non-ideal (e.g. organic vapors). On the one hand, the reference case using air at 5 bar is shown, where its ideal-gas behavior can be noted (Z=1). On the other hand, the propane and isobutane operating points provide a significant variation of $Z \neq f(s)$ along the isentropic compression line. This means that the selected conditions are closer to a non-ideal gas than to an ideal vapor behavior. However, their closeness to the perfect-vapor behavior $Z = f(s)$ has to be assessed through the influence of the $\partial Z/\partial p|_s$ partial derivative. In addition, it is interesting to note the fact that although isobutane points provide Z values not as low as propane, a higher derivative may be observed.

Furthermore, non-ideal compressible fluid dynamics can be evaluated through the evolution of the local speed of sound thermophysical property. Figs. 4(a) and 4(b) show the speed of sound contours for the operating points studied. Absolute value variations are clearly found, being larger near the saturation line, which must be taken into account for the dynamical similitude analysis, especially when dealing with the isentropic head rise. In addition, one may observe that iso-speed of

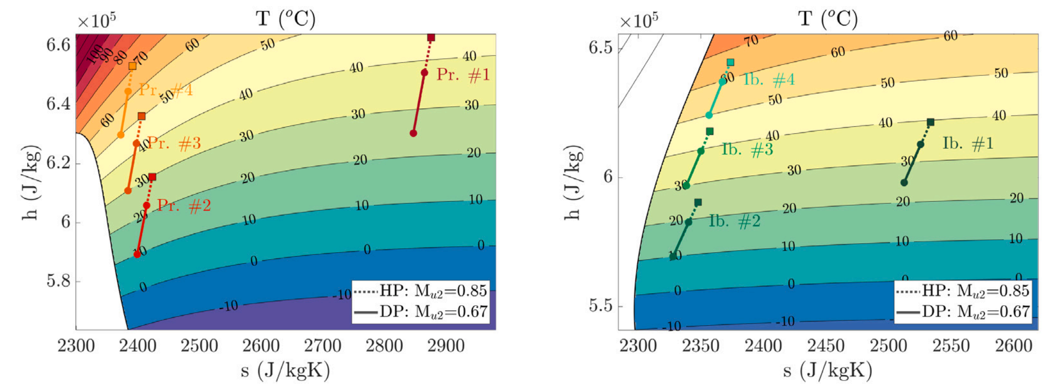

(a) Propane (b) Isobutane

Fig. 2. Temperature contours on an enthalpy-entropy diagram for both organic fluids. The resulting compression lines for the set of operating points studied are marked and labeled. The solid lines represent the DP and the extended dotted lines HP performance operation.

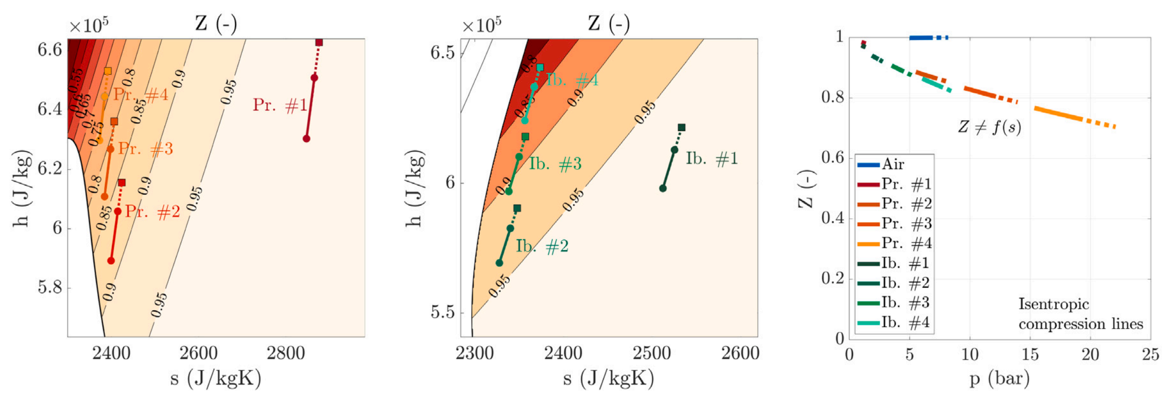

(a) Propane (b) Isobutane (c) Comparison

Fig. 3. Polytropic compression lines over the compressibility factor contours (a, b) and their evolution at isentropic compression lines over the pressure evolution. The solid lines represent the DP and the extended dotted lines HP performance operation.

sound lines provide regions with positive, near 1 and, negative gradient in comparison to the compression process. In fact, the fundamental derivative of gas dynamics Γ provides a value precisely according to the speed of sound variation along with the variation of the pressure. Γ values above 1 implies a positive $\partial a/\partial p|_s$ derivative, entailing a perfect gas behavior. Conversely, negative $\partial a/\partial p|_s$ derivative provide $\Gamma < 1$ values. These fluids are called non-ideal dense gases or dense vapors in the range of $0 < \Gamma < 1$. In order to see this evolution on the selected operating points, Fig. 4(c) represents the variation in the speed of sound at the selected compression lines where its decrease along the compression features non-ideal effects. The operating points Pr. #2–4 and Ib. #2–4 feature a fundamental derivative Γ below 1 (in the range of 0.88–0.98). The closer the critical region and the saturation line is, the lower the value of Γ. One may also note a lower variation using the organic vapors than using air, which may ease the dynamical similarity behavior preservation.

4. Results

The results section is structured as follows: first, the analytical results obtained through the proposed generalized similarity-based methodology are shown; next, numerical results are analyzed to validate dynamical similarity preservation; finally, averaged numerical key indicators are compared with analytical indicators to understand the source of deviations when scaling to organic fluids.

4.1. Dynamical similitude analysis for the selected operating points

This first subsection analyzes the results applying dynamical similarity conditions using the upgraded generalized flow method presented in this work. The set of study consists of sixteen different operating points using organic fluids and, additionally, their homologous air reference cases. According to the compressor performance, two different compressions are analyzed: a lower pressure ratio line (DP) with a peripheral Mach number (M_{u2}) of 0.67 and a larger pressure ratio compression line (HP) that provides an increased temperature lift, with a M_{u2} of 0.85. At these conditions, the resultant dimensionless mass flow rate is 0.043 for DP and 0.061 for HP while the blade Mach number is 0.272 and 0.214, respectively. Keeping dynamical similarity while varying the working fluids (Pr./Ib.) and heat pump-based pressure/temperature conditions (#1–#4) leads to both an isentropic stage loading coefficient and a theoretically polytropic efficiency constant. It is worth noting that the Reynolds number for all the points studied is larger than 10^5.

Under these conditions, the modified Eckert and Traupel numbers can be computed. It is worth recalling that these dimensionless numbers are not imposed so that their variation and influence on dynamical similitude can be further assessed. Fig. 5(a) shows ($Ec^{*1/2}$) values for all the set at both HP and DP compressor performances. One may note a decrease in Eckert while moving the compression line closer to the critical region as a consequence of an increase in the compressor inlet pressure. This is why Pr. #4 and Ib. #4 provide the lowest values. Slight deviations are also observed between the propane and isobutane operating points. Furthermore, proportional trends are observed between HP and DP. Global deviations from −20% to −44% are found in comparison to the air reference case, although absolute values remain in the range 0.18–0.32. Numerical validation is required to determine the degree of dependence of this dimensionless number on similitude.

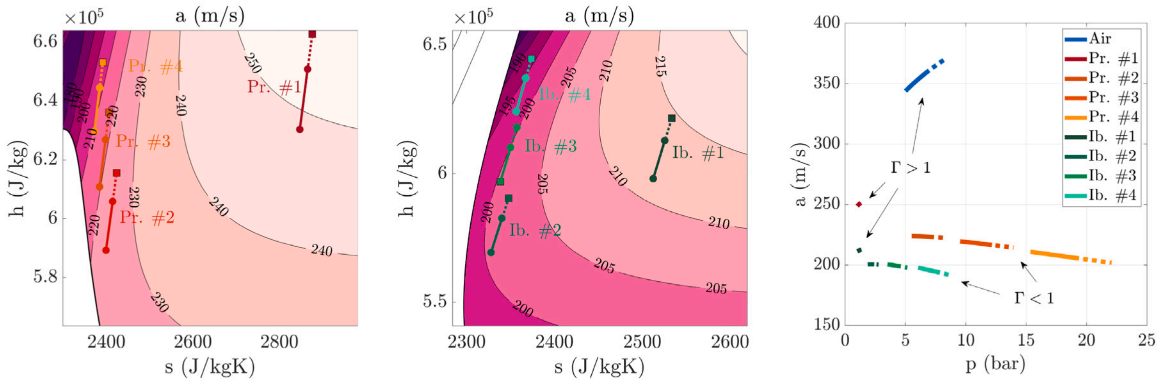

(a) Propane (b) Isobutane (c) Comparison

Fig. 4. Polytropic compression lines over the local speed of sound contours (a, b) and comparison along the pressure evolution. The solid lines represent the DP and the extended dotted lines HP performance operation.

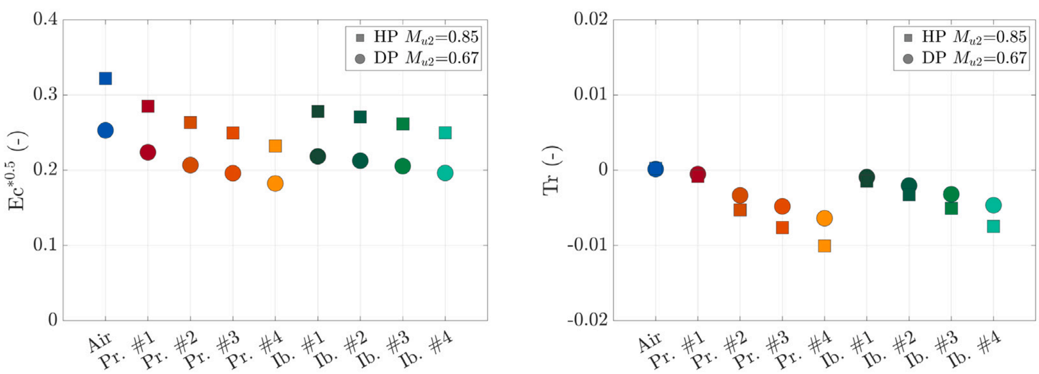

(a) (b)

Fig. 5. (a) Modified Eckert and (b) Traupel number variations along the selected organic operating points and the reference air case.

Similarly, the Traupel number values are shown in Fig. 5(b). Negative near-zero *Tr* values are obtained due to the negative compressibility factor slope along the organic compressions. It is interesting to highlight that despite these notable slopes shown in previous Fig. 3(c), the factor driven by the rotational speed, density and characteristic dimension ($\rho n^2 D^2$) is not large enough to obtain a non-zero *Tr*. For example, the first factor of *Tr* in Pr. #3 operating point is 4.4 $\cdot 10^4$, while its compressibility factor slope is $-1.1 \cdot 10^{-7}$. A double rotational speed and five times the inlet density would be needed to obtain a *Tr* around −0.1. This means that, at present subsonic Mach conditions (< 0.6–0.75), the Traupel effect on non-ideal flow dynamics can be neglected and its role on similitude dimensionless number is dismissed for the proposed organic vapors under these heat pump conditions. This also means that the flow dynamics may be more comparable to the perfect vapor behavior.

Finally, the resultant total-to-total pressure ratios applying dynamical similitude are shown in Fig. 6(a). Notable reductions are found in comparison to the reference case, being larger at HP compressor performance. This is because the absolute difference in the speed of sound of both organic fluids in comparison to air reduces the enthalpy rise while isentropic head coefficients are kept. Therefore, the compressions of organic vapor under heat pump conditions can be cut to a 14%. Fig. 6(b) shows the variations in the total-to-total density ratio. It is interesting to note that these deviations start to be important under HP compressor performance (increased pressure ratio), while at the DP they seem to be within a reasonable band. These alterations might affect flow field similitude, so numerical validation is required to analyze the influence of these differences on both the global flow field and to the key performance indicators.

4.2. Numerical validation

This subsection aims to prove that dynamical similarity is achieved in numerical simulations through the inputs generated by the proposed generalized scaling laws. First, the averaged velocities at representative stage stations are studied. Fig. 7 depicts the numerically-obtained mass flow averaged absolute Mach (*Ma*) and relative Mach (Ma_w) numbers along the compressor stage in terms of relative difference compared to the reference air case.

The operating points under DP compressor performance (Fig. 7(a)) show an average discrepancy of ±2.5%, which is a reasonably good Mach agreement, especially across the impeller. This may confirm that the homologous conditions provided by analytical scaling entail that dynamical similarity conserves the dominant flow Mach numbers. A non-ideal-behavior-driven pattern is found, where operating points #3 and #4 provide a light increase in deviation, magnified at the diffuser outlet. Relative differences for HP compressor performance can be observed in Fig. 7(b). Although the deviations at the inlet and near the leading edge remain in the same band, the error at the impeller outlet and diffuser outlet stations increases around the 5% band. Moreover, the farthest operating point from ideal conditions shows an intensified deviation, which rises up to 10% at the diffuser outlet, driven by the previously detected non-ideal behavior pattern. It is interesting to note that these deviations at the outlet are related to modifications in the total-to-total density ratio. The increase in outlet density leads to higher Mach numbers if the geometry is unaltered. As explained previously, this situation escalates at higher pressure ratios (HP vs. DP). Therefore, both the global flow field analysis and its further influence on key performance indicators is required in order to assess whether

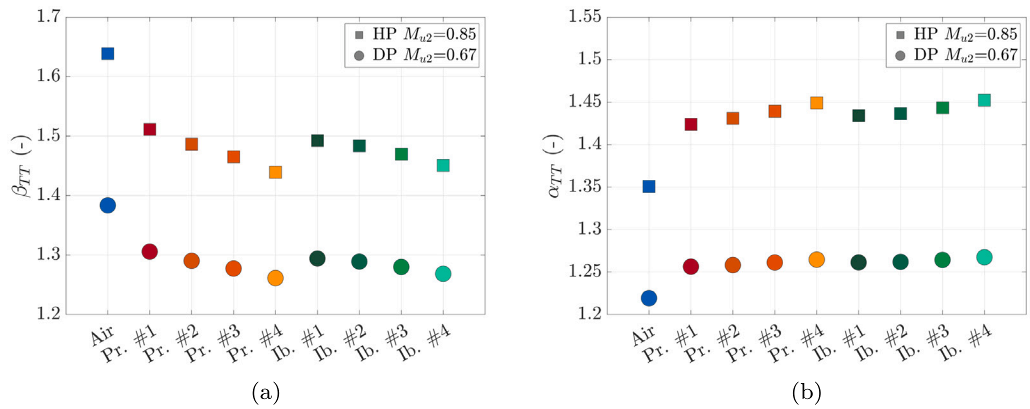

Fig. 6. Resulting (a) total-to-total pressure ratio and (b) total-to-total density ratios after applying the similarity-based methodology along the selected organic operating points and the reference air case.

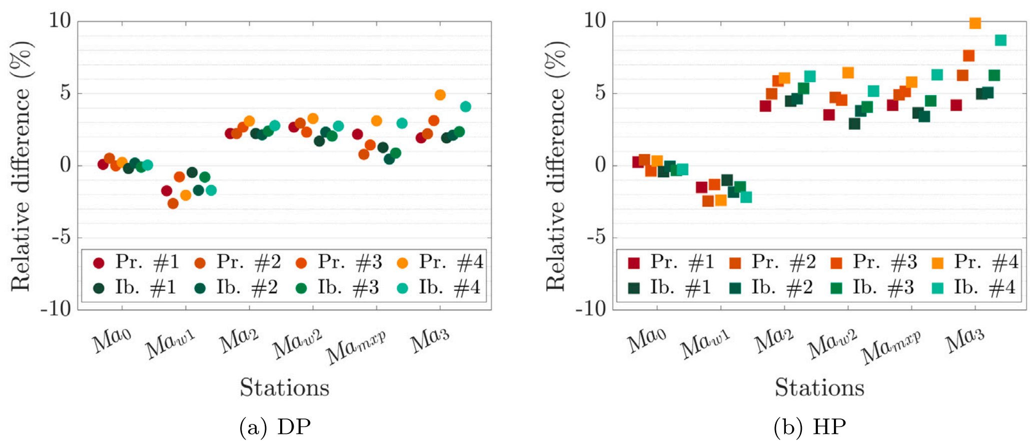

Fig. 7. Absolute (*Ma*) and relative (Ma_w) mass flow averaged Mach number relative difference vs air reference case at different stations for both compressors operating points: (a) DP and (b) HP [0: inlet, 1: near impeller leading edge, 2: near impeller trailing edge, mxp: mixing plane, 3: diffuser outlet].

these differences are permissible to guarantee dynamical similarity preservation.

The global flow field structures are compared hereafter. Two organic operating points under HP compressor performance using propane at the highest inlet pressure (Pr. #4) and isobutane at the lowest (#Ib. 1) are selected to verify that not only averaged Mach numbers are preserved, but also the velocity flow field structures. Fig. 8(a) shows the absolute and relative Mach number contours on stage blade-to-blade view at half span location for the reference air operating point. Then, the fluid flow fields corresponding to operating points Pr. #4 and Ib. #1 are shown in Figs. 8(b) and 8(c), respectively.

One may observe a similar main flow structure along the impeller section. The transition between absolute and relative Mach number is properly characterized at the compressor inlet leading to similar incidences at the main blade leading edge. The discrepancies of the averaged computed incidence are in the order of ±0.4°. Near-wall velocity gradients of both pressure and suction sides of the blades are maintained. Furthermore, the same tip-leakage-induced bubble structure at the trailing edge suction side is found. Similarly, trailing edge deviations remains at ±0.2°. This qualitative comparison contributes to the assurance of homologous working conditions on the studied organic vapor compressions.

The last step to accomplish the numerical validation is to evaluate the dynamical similitude in terms of key performance indicators. Fig. 9 shows the relative difference between the numerically-obtained parameters and those obtained through the proposed similarity-based methodology. One may note that isentropic head coefficient deviations (Fig. 9(a)) result in a reduced band of ±2.5% compared to Mach number differences. In addition, non-ideal behavior patterns do not seem to convey increased deviations. Meanwhile, Fig. 9(b) shows polytropic efficiency differences, which are generally overestimated by 2% without identifying a clear trend. Therefore, numerical results can validate the proposed scaling methodology within these reduced error bands under the heat pump conditions of this work. Finally, it is interesting to analyze the most characteristic performance indicator of a compressor: the total-to-total pressure ratio. Fig. 9(c) collects the deviations when dealing with the organic fluids selected under different heat pump conditions. A good agreement between both methods is obtained with a reduced error band in the range of ±1%, being even lower at HP compressor performance. The good prediction of the pressure ratio, as a final step, allows the generalized flow method to be validated with a significant degree of prediction in spite of the non-ideal fluids.

4.3. Non-ideal influence on key performance indicators

Once similitude is numerically proven for the selected organic vapors conditions, it is interesting to analyze the analytical-numerical deviations on key performance indicators and the emerging trends between different indicators and characteristic non-ideal thermophysical properties or the modified Eckert dimensionless numbers. Isentropic head coefficient and polytropic efficiency are analyzed in Fig. 10. Figs. 10(a)–10(b) show the influence of the compressibility factor and the real isentropic pressure-volume exponent on the head coefficient, respectively, through a scatter plot which depicts the comparison between the results obtained using the proposed analytical dynamic similitude method (DS) and using the numerical model (CFD) for all the

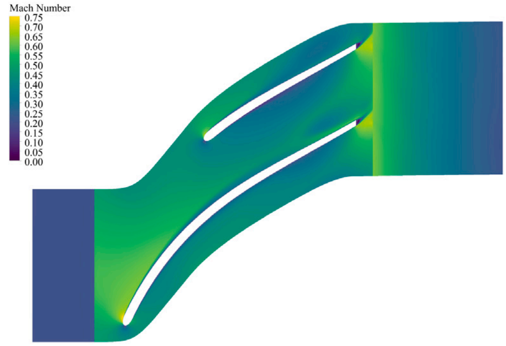

(a) Air

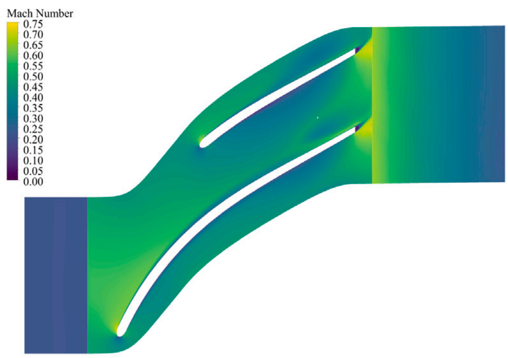

(b) Propane #4

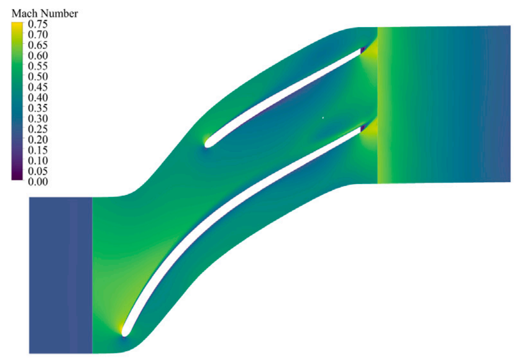

(c) Isobutane #1

Fig. 8. Mid-span blade-to-blade view of stationary and relative Mach number fields for two selected operating points at organic vapor conditions and for the reference air case.

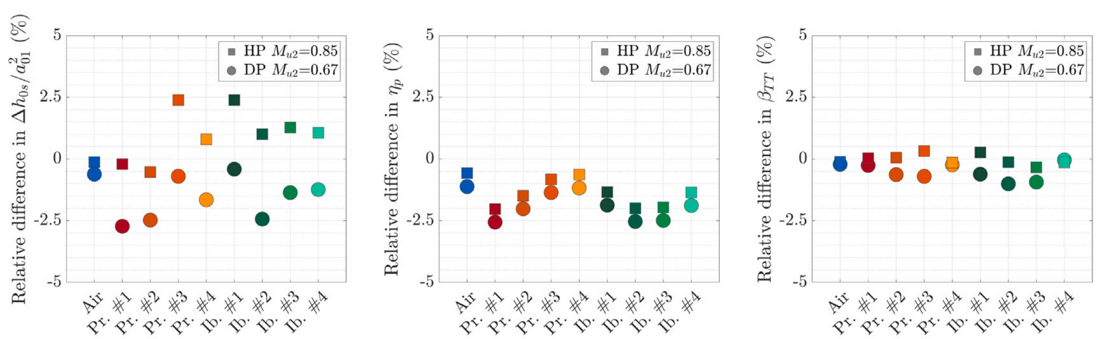

(a) (b) (c)

Fig. 9. Relative difference between numerical and similarity results for (a) isentropic head coefficient, (b) polytropic efficiency and (c) total-to-total pressure ratio.

operating points, including the reference air case. Deviations between DS and CFD results do not form identifiable patterns. This means that their deviations could not be followed by Z and γ_{pv}. A similar study on polytropic efficiency is conducted in Figs. 10(d)–10(f). These scatter charts depict the distribution of the previously detected 2% overestimation according to DS. No patterns along Z or γ_{pv} can be identified in these deviations, which throw good matches far from ideal behavior. In other words, these discrepancies in both isentropic head coefficient and efficiency are not caused by the organic vapor non-perfectness itself, since good matches can be found at high and low Z and γ_{pv}.

Regarding dimensionless numbers considered in the proposed generalized flow similarity-based method, one may recall that variations in the Traupel number cannot be responsible for those variations due to their negative near-zero value in all the operating points set ($-0.01 < Tr < 0$). This means that perfect vapor-like behavior may be expected under these conditions. Therefore, the alterations in the other dimensionless number (the modified Eckert number) are studied in Figs. 10(c) and 10(f). Similarly, there is no evidence to devise a clear effect of the Eckert number on both $\Delta h_{0s}/a_{01}^2$ and η_p. Hence, it cannot be stated that the variations on this new dimensionless number in the range of 0.18–0.22 and 0.23–0.29 for the corresponding reference cases (0.25 and 0.32) convey an impact on both similitude key performance indicators. Overall, one may find a notable good agreement between both methods according to the assessment of the two indicators involved, thus the scaling analysis works, attributing the main cause of deviations to numerical error.

Finally, the resultant key parameter total-to-total pressure ratio is analyzed in Fig. 11. It is worth recalling that this indicator is not fixed in the similarity-based scaling method, being computed afterwards.

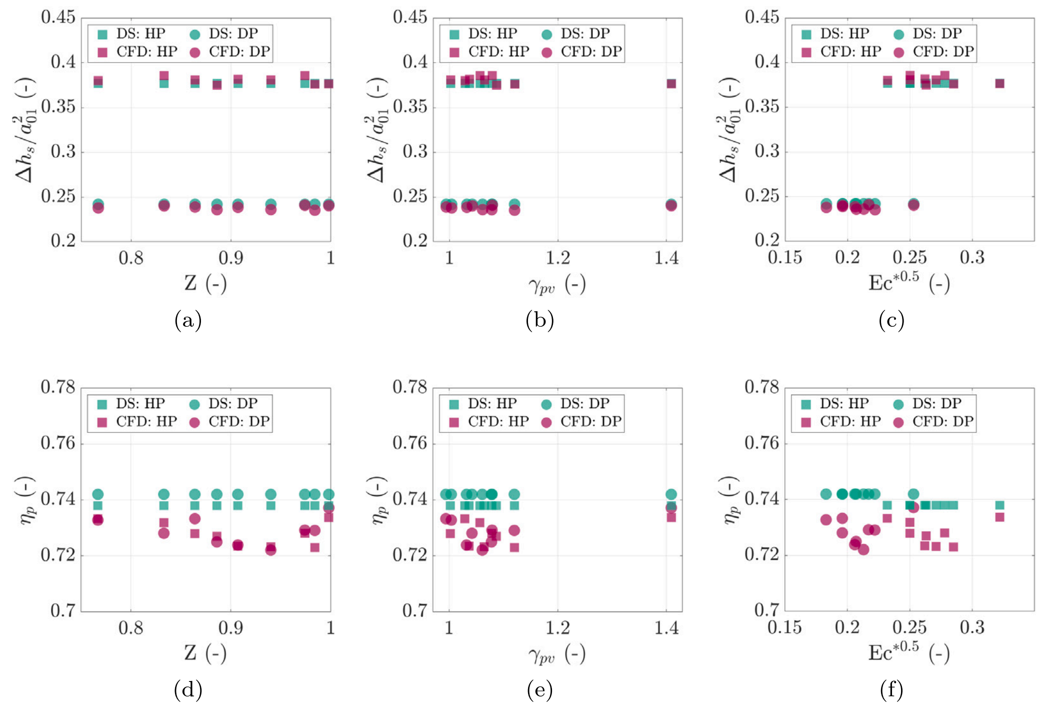

Fig. 10. Scatter plots of (a–c) isentropic head coefficient and polytropic efficiency (d–f) vs. thermophysical properties (Z and γ_{pv}) and modified Eckert number for the set of operating points comparing dynamical similitude (DS) calculations and numerically obtained (CFD) results.

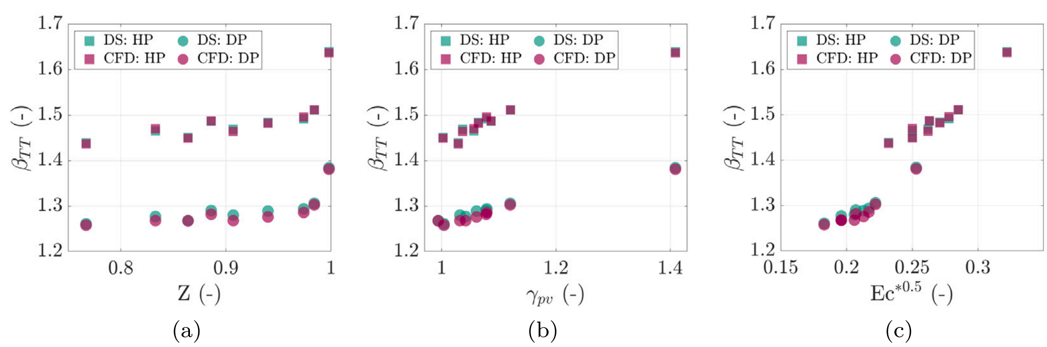

Fig. 11. Scatter plots of total-to-total pressure ratio vs. thermophysical properties (Z and γ_{pv}) and modified Eckert number for the set of operating points comparing dynamical similitude (DS) calculations and numerically obtained (CFD) results.

Its relationship between Z and γ_{pv} is shown in Figs. 11(a)–11(b). A clear trend with the compressibility factor is devised, following an exponential line which notably increases near Z=1. In addition, there is also a clear evolution with γ_{pv}, where a quasi-linear regression may be obtained. These patterns are clearly identified at both HP and DP compressor performances, providing consistency in the results obtained. It is interesting to highlight the notable precision in the total-to-total pressure ratio prediction when comparing to CFD results, even though Z and γ_{pv} are not explicitly considered as independent dimensionless groups in the scaling method. In other words, Z and γ_{pv} effects on β_{TT} are captured without establishing an explicit dependency.

Fig. 11(c) shows the modified Eckert number relationship with total-to-total pressure ratio where a clear evolution can easily be devised. Since the proposed similarity-based methodology does not keep this indicator constant, this dependency is allowed and there is no need for additional corrections to the method. Scaling results provide enough accuracy in comparison to CFD results that also provide the same patterns. All in all, the proposed generalized flow scaling method achieves a remarkable pressure ratio prediction when dealing with organic vapor compressions under these low-temperature lift turbomachinery-based heat pumps including non-ideal flow dynamics effects.

5. Conclusions

The present study investigates the prediction ability of a similarity-based method proposed for generalized behavior fluids dynamics in turbomachinery. Hence, a non-ideal effects assessment is performed in order to provide its applicability. Due to the increasing interest in turbomachinery-based heat pump-based applications, this study is carried out using organic vapors at different operating conditions near the saturation line, compressed by a high-speed small radial turbocompressor. In light of the results of this paper, the following findings can be drawn:

- The updated version of the generalized flow turbomachinery dynamic similarity method proposed in this work provides a proper performance with a formal consideration of the behavior of two non-ideal working fluids working close to the saturation line, including implicit variations on compressibility factor and real isentropic pressure-volume exponent.
- Dynamical similarity conditions are numerically checked through averaged Mach numbers across the stage but also along the velocity flow fields. Allowed deviations are linked to the resultant

variation in the density ratio, which is maintained in order not to modify the geometry. Key performance deviations are in the range of ±2.5% for the isentropic head rise, while polytropic efficiency is overestimated by a 2% and total-to-total pressure ratio prediction remains within a ±1%. Therefore, a numerical validation is achieved at this notable level of agreement.
- The set of operating points at different heat pump conditions, temperature lifts using two different organic vapors (propane and isobutane) working with the reference micro-scale turbocompressor provide near-zero Traupel numbers. Variations in the range of $-0.01<Tr<0$ do not demonstrate any substantial effect. Therefore, perfect vapor-like behavior can be assumed and Traupel number is not required at these conditions to maintain the dynamical similarity, despite being close to the saturation line with both compressibility factor and fundamental derivative of gas dynamics below 1.
- Regarding the modified Eckert number, slight variations are found although both the isentropic stage loading and polytropic efficiency are not affected at the studied variation in modified Eckert number. Further data need to be reported to correctly assess its suitability and range of influence.
- The prediction of the total-to-total pressure ratio through the proposed scaling method is well achieved in comparison with numerical simulation considering the non-ideal behavior of the working fluids under the heat pump conditions studied in this work. Hence, it is interesting to highlight that this advantageous region at the study conditions close to the saturation line may allow the use of scaling laws for heat pump designs without an additional need for Eckert and Traupel number corrections.

This study has confirmed the suitability of the scaling method for high-speed radial small turbocompressors operating near the saturation line (where heat pump-based systems work) when using propane and isobutane without the need for additional corrections. Despite the high rotational speed, the near-zero Traupel number leads one to assume perfect vapor behavior. One may wonder when these assumptions cannot be extended. On this basis, the next step will be to study small compressors providing higher pressure ratios per stage (or using other working fluids), to fulfill increased temperature lifts for heat pump-based applications. However, multistage turbocompressors may address this issue, which also entails interesting work to conduct in terms of concept design. Furthermore, the notable focus on high-temperature heat pumps makes it also interesting to study scaling methods when more relevant non-ideal flow effects dominate. Experimental future works will also shed some light to address attractive comparisons with real data of organic vapor compressions.

CRediT authorship contribution statement

Andrés Sebastián: Conceptualization, Methodology, Visualization, Writing – original draft. **Rubén Abbas:** Conceptualization, Supervision, Writing – review & editing. **Manuel Valdés:** Conceptualization, Supervision, Writing – review & editing.

Declaration of competing interest

The authors declare that they have no known competing financial interests or personal relationships that could have appeared to influence the work reported in this paper.

Acknowledgments

This research has been supported by the Spanish *Ministerio de Ciencia e Innovación* under the project reference number PID2019-110283RB-C32.

Data availability

Data will be made available on request.

References

[1] Gaur AS, Fitiwi DZ, Curtis J. Heat pumps and our low-carbon future: A comprehensive review. Energy Res Soc Sci 2021;71:101764.
[2] Kou X, Wang R, Du S, Xu Z, Zhu X. Heat pump assists in energy transition: Challenges and approaches. DeCarbon 2024;3:100033.
[3] Schiffmann J, Favrat D. Design, experimental investigation and multi-objective optimization of a small-scale radial compressor for heat pump applications. Energy 2010;35(1):436–50.
[4] Arpagaus C, Bless F, Uhlmann M, Schiffmann J, Bertsch SS. High temperature heat pumps: Market overview, state of the art, research status, refrigerants, and application potentials. Energy 2018;152:985–1010.
[5] Garland SD, Noall J, Bandhauer TM. Experimentally validated modeling of a turbo-compression cooling system for power plant waste heat recovery. Energy 2018;156:32–44.
[6] Sebastián A, Abbas R, Valdés M, Rovira A. Modular micro-trigeneration system for a novel rotatory solar Fresnel collector: A design space analysis. Energy Convers Manage 2021;227:113599.
[7] Steinmann W-D, Bauer D, Jockenhöfer H, Johnson M. Pumped thermal energy storage (PTES) as smart sector-coupling technology for heat and electricity. Energy 2019;183:185–90.
[8] Steger D, Regensburger C, Eppinger B, Will S, Karl J, Schlücker E. Design aspects of a reversible heat pump - Organic rankine cycle pilot plant for energy storage. Energy 2020;208:118216.
[9] Burnand GP-A. Small scale very high speed slotless permanent magnet motors (Ph.D. thesis), EPFL; 2020.
[10] Casey M, Krähenbuhl D, Zwyssig C. The design of ultra-high-speed miniature centrifugal compressors. In: Proceedings of the 10th European conference on turbomachinery, fluid dynamics and thermodynamics. 2013.
[11] Wiesche Sad. Experimental investigation techniques for non-ideal compressible fluid dynamics. Int J Turbomach, Propul Power 2023;8(2).
[12] Macchi E, Astolfi M. Organic rankine cycle (ORC) power systems: technologies and applications. Woodhead Publishing; 2016.
[13] Romei A, Vimercati D, Persico G, Guardone A. Non-ideal compressible flows in supersonic turbine cascades. J Fluid Mech 2020;882:A12.
[14] Baumgärtner D, Otter JJ, Wheeler AP. The effect of compressibility factor on turbine performance. In: Turbo expo: power for land, sea, and air, vol. 84966. American Society of Mechanical Engineers; 2021, V004T06A020.
[15] Giuffre' A, Pini M. Design guidelines for axial turbines operating with non-ideal compressible flows. J Eng Gas Turbines Power 2021;143(1):011004.
[16] aus der Wiesche S, Reinker F. Dimensional analysis and performance laws for organic vapor flow turbomachinery. Energy 2022;257:124635.
[17] Meroni A, Zühlsdorf B, Elmegaard B, Haglind F. Design of centrifugal compressors for heat pump systems. Appl Energy 2018;232:139–56.
[18] Van den Braembussche R. Design and analysis of centrifugal compressors. John Wiley & Sons; 2019.
[19] Casey M, Robinson C. Radial flow turbocompressors. Cambridge University Press; 2021.
[20] Jeong Y, Son S, Cho SK, Baik S, Lee JI. Evaluation of supercritical CO2 compressor off-design performance prediction methods. Energy 2020;213:119071.
[21] Zou Z, Ding C. A new similarity method for turbomachinery with different working media. Appl Therm Eng 2018;133:170–8.
[22] Valdés M, Sebastián A, Abbas R. Reynolds-number-dependent efficiency characterization of a micro-scale centrifugal compressor using non-conventional working fluids. Energy Convers Manage 2018;177:224–32.
[23] Sebastián A, Abbas R, Valdés M. Analytical prediction of Reynolds-number effects on miniaturized centrifugal compressors under off-design conditions. Energy 2021;227:120477.
[24] Sebastián A, Abbas R, Valdés M. Effect of pressurization on tip leakage losses in micro-scale centrifugal compressors. In: Proceedings of the 14th European conference on turbomachinery, fluid dynamics and thermodynamics. April 12-16.
[25] Tosto F, Lettieri C, Pini M, Colonna P. Dense-vapor effects in compressible internal flows. Phys Fluids 2021;33(8).
[26] Giuffre A, Colonna P, Pini M. The effect of size and working fluid on the multi-objective design of high-speed centrifugal compressors. Int J Refrig 2022;143:43–56.
[27] Rusch D, Casey M. The Design Space Boundaries for High Flow Capacity Centrifugal Compressors. J Turbomach 2013;135(3):031035.
[28] Dixon S, Hall C. Chapter 2 - dimensional analysis: Similitude. In: Dixon S, Hall C, editors. Fluid mechanics and thermodynamics of turbomachinery. seventh ed. Boston: Butterworth-Heinemann; 2014.
[29] Lemmon EW, Bell I, Huber ML, McLinden MO. NIST Standard Reference Database 23: Reference Fluid Thermodynamic and Transport Properties-REFPROP, Version 9.0, National Institute of Standards and Technology. 2010.

[30] Sebastián A, Abbas R, Valdés M. Experimental investigation of key aerothermal phenomena in micro-scale radial turbocompressors. Therm Sci Eng Prog 2023;39:101748.

[31] Celik IB, Ghia U, Roache PJ, Freitas CJ, Coleman H, Raad PE. Procedure for estimation and reporting of uncertainty due to discretization in CFD applications. J Fluids Eng-Trans ASME 2008;130(7). 078001–078001–4.

[32] Liu H, Zhao B, Zhang Z, Li H, Hu B, Wang R. Experimental validation of an advanced heat pump system with high-efficiency centrifugal compressor. Energy 2020;213:118968.

[33] Jaatinen-Värri A, Honkatukia J, Uusitalo A, Turunen-Saaresti T. Centrifugal compressor design for high-temperature heat pumps. Appl Therm Eng 2024;239:122087.

[34] Jiang J, Hu B, Ge T, Wang R. Comprehensive selection and assessment methodology of compression heat pump system. Energy 2022;241:122831.

[35] Gasser L, Flück S, Kleingries M, Meier C, Bätschmann M, Wellig B. High efficiency heat pumps for low temperature lift applications. In: Proceedings of the 12th IEA heat pump conference. 2017, O.1.4.5.

[36] Traupel W. Thermische turbomaschinen: Erster band thermodynamisch-strömungstechnische berechnung. Springer Berlin, Heidelberg; 1977.